Design and Fabrication of Flexible Capacitive Sensor With Cellular Structured Dielectric Layer via 3D Printing

Wenzhen Yang, Yu Liu, Wei Xu, and Heng-Yong Nie

***Abstract*—Because of high sensitivity, mechanical robustness, lightweight and wearability, flexible capacitive pressure transducer has been widely considered one of the most critical soft electronics in wearable consumables and e-skins. The enhancement of the pressure sensitivity of a flexible capacitive sensor relies on the introduction of interfacial microstructure to the dielectric layer. We demonstrate a new methodology to fabricate flexible capacitive sensors with copper-plated polyimide (PI) films as the electrodes and a porous polydimethylsiloxane (PDMS) layer 3D printed via the direct-ink-writing approach. Time-of-flight secondary ion mass spectrometry is developed to optimize the electroless copper plated PI films. What is further examined is the impact of the geometric complexity of the cellular PDMS structure, including filament width, spacing and alignment, on sensitivity, repeatability and reliability of the developed capacitive sensor. A robotic gripper equipped with our flexible pressure sensor showcases its competence to grip a soft target with well-posed force control. It is expected that our proposed sensor design and manufacturing methodology will advance the development of soft electronics and wearable sensors.**

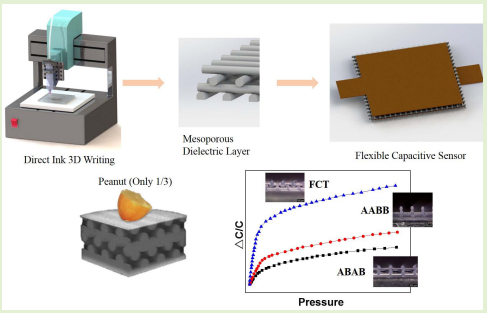

***Index Terms*— Flexible capacitive pressure sensor, cellular structure, 3D printing, sensitivity, dielectric layer.**

I. Introduction

FLEXIBLE electronics represent one of the essential advances in the development of next-generation electronic devices, which have been becoming increasingly popular in soft robotics, wearable human healthcare, and electronic skin [1]–[5]. More specifically, flexible pressure sensors, in contrast to its traditional counterparts based on a rigid silicon substrate, conform to complex geometric surfaces and transduce their haptic stimuli to electrical signals [6], [7]. The flexible pressure sensors can retain their electrical behaviors under different forms of deformation, such as bending, twisting, and stretching [8], [9]. Upon external mechanical stimuli, capacitive sensors gain the primary competence in detecting both dynamic and static loads among resistive, piezoelectric, triboelectric or capacitive sensing modes [10], maintaining high measuring sensitivity, robustness to temperature and humidity, and compact circuit layout design [11], [12].

For a flexible capacitive pressure sensor, the modification of the dielectric constant and elasticity modulus of the dielectric layer and electrode is able to enhance its performance (sensitivity). Bao's group [12], [13] led the work via photolithography for the preparation of a pyramid-like microstructure on a thin elastomeric polydimethylsiloxane (PDMS) dielectric layer. Their flexible capacitive sensors with the microscale features exhibited a sensitivity 30 times higher than the unstructured counterpart. Recently, numerous studies have been reported on synthesizing polymeric dielectric layers with micro-composite structures and/or nano-composite structures of microporous [14]–[16], microporous pyramid [17]–[19], micro pyramid [20], microhair [21],

Manuscript received December 12, 2020; revised February 6, 2021; accepted February 9, 2021. Date of publication February 18, 2021; date of current version April 5, 2021. This work was supported in part by the National Natural Science Foundation of China under Grant 51875253 and in part by the Fundamental Research Funds for the Central Universities under Grant JUSRP21910. The associate editor coordinating the review of this article and approving it for publication was Dr. Shyqyri Haxha. *(Wenzhen Yang and Yu Liu contributed equally to this work.) (Corresponding authors: Yu Liu; Heng-Yong Nie.)*

Wenzhen Yang is with the School of Mechanical Engineering, Jiangnan University, Wuxi 214122, China.

Yu Liu is with the School of Mechanical Engineering, Jiangnan University, Wuxi 214122, China, and also with the Jiangsu Key Laboratory of Advanced Food Manufacturing Equipment and Technology, Jiangnan University, Wuxi 214122, China (e-mail: yuliu@jiangnan.edu.cn).

Wei Xu was with the School of Mechanical Engineering, Jiangnan University, Wuxi 214122, China. He is now with Schneider Electric, Wuxi 214028, China.

Heng-Yong Nie is with the Surface Science Western, The University of Western Ontario, London, ON N6G 0J3, Canada, and also with the Department of Physics and Astronomy, The University of Western Ontario, London, ON N6A 3K7, Canada (e-mail: hnie@uwo.ca).

This article has supplementary downloadable material available at https://doi.org/10.1109/JSEN.2021.3060281, provided by the authors.

Digital Object Identifier 10.1109/JSEN.2021.3060281

microdome [22], micro-convex [23] and micropillar [24]. Joo *et al.* had designed a silver, nanowire-embedded PDMS electrode with a multiscale structure to tune the performance of their pressure sensors [25].

Despite having achieved significantly improved pressure sensitivity, the micropatterning processes still suffer from a series of issues, such as time-consuming complexity, limited scalability, and/or less compatibility with more universal materials [26]. Recent advances in the field demonstrated that soft cellular polymer structures emerged to be innovative constitutes of highly sensitive pressure sensors [27], [28]. The work of Pruvost *et al.* presented a capacitive sensor consisted of a low modulus, high dielectric constant composite foam and coated carbon black, with enhanced device sensitivity of 35 kPa^{-1} in 0 to 0.2 kPa and 6.6 kPa^{-1} in 0.2 to 1.5 kPa [29]. The sensitivity of the microstructured porous pyramid-based pressure sensor developed by Yang *et al.* is as high as 44.5 kPa^{-1} in 0-0.1 kPa [18]. By forming a porous elastomer as the dielectric layer and using conductive fabric as the electrodes, a capacitive sensor is developed with a sensitivity of 0.0121 kPa^{-1} and measurement range up to 100 kPa [27]. Wan *et al.* directly used natural plant petal as a dielectric layer, in which the 3D cell wall meshed from the plant surface provides the same effect as compressible materials [30]. This method led to a maximum sensitivity of 1.54 kPa^{-1}. However, these existing methods are hardly a controlled process to produce an elastomeric dielectric layer with microstructure, which leads to rather poor reproducibility.

For fabrication of cellular dielectric materials, 3D printing is being widely considered as an efficient and scalable technique being capable of orderly structuring feature sizes at the micro and nanometer scales [31]. The direct ink writing (DIW), via layered deposition of continuous wet filaments [32]–[34], is especially suitable to prepare elastic foam with controlled, multiscale lattice structures in a low-cost, environment-friendly and precise manner. Several groups [35]–[37] have led many decisive exertions on the design and fabrication of functional elastomeric cellular materials by DIW, revealing that different structures could tune the mechanics of porous cushions. We report in this article the first attempt to utilize DIW 3D printing as a direct, scalable manufacturing method to form PDMS cellular dielectric layers. Integrated with flexible electrodes prepared by electroless plating of copper on polyimide (PI) thin films [38], a flexible capacitive pressure sensor with high sensitivity can be easily manufactured. The mechanical controllability of the cellular PDMS will be comprehensively discussed for revealing our new findings.

II. Experimental Section

A. Materials

For DIW of elastomeric filaments, a DOWSIL™ SE 1700 Silicone Elastomer kit containing PDMS and curing agent was purchased from Dow Corning. The PDMS structure used as the dielectric layer of the flexible capacitive sensor was 3D printed on a silicon wafer that was cleaned using deionized water and followed by rinsing with a 1 wt% trichloro (1H, 1H, 2H, 2H-perfluorooctyl) silane solution in alcohol. This surface modification renders the silicon wafer hydrophobic, which assists to release the 3D printed PDMS structure more easily. PI films with an electroless plated copper layer were used as the flexible electrodes of the capacitive sensor. The chemicals used for the electroless plating bath and the detailed plating processing were described elsewhere [38]. Before electroless plating of copper, the PI films were activated with NaOH followed by catalyzation with silver via immersion in a solution of silver nitride ($AgNO_3$) in a mixture of de-ionized water and ethanol.

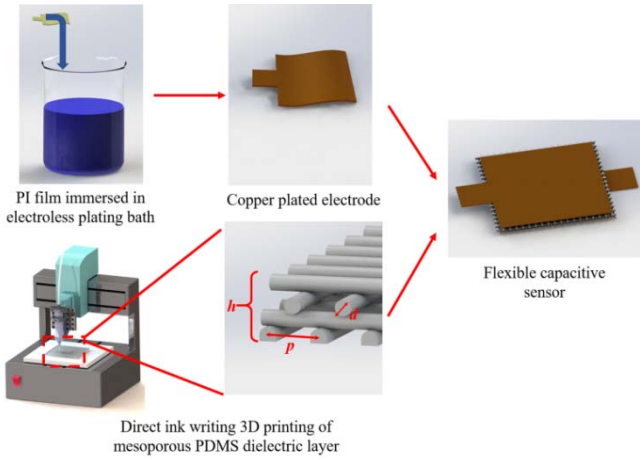

Fig. 1. Schematics of the fabrication of a flexible capacitive sensor involving electroless plating of copper on polyimide films as electrodes and 3D printing of a dielectric PDMS structure of stacked filaments.

B. Fabrication of Flexible Capacitive Sensor

The fabrication process was shown in Fig.1 and implemented on a homemade DIW 3D printer, consisting of a computer-controlled 3-axis gantry platform. A pneumatic dispenser modified with a high-pressure booster was mounted on the printer to print the PDMS ink in high spatial resolution. As illustrated in Fig. 2, mesoporous dielectric layers with desired architectures were fabricated by controlling the deposition of the PDMS ink along the defined printing paths. Letter A denotes a 3D printed meandering filament, while B represents a filament rotating 90° from A. The four layers of 3D printed PDMS filament stacked as an AABB structures, with the first layer printed on a support (e.g., surface modified silicon wafer) being A, is shown in Fig. 2a. The cross section is also illustrated in the figure. An ABAB structure is shown in Fig. 2b. As shown in Fig. 2c, with the 3rd layer being shifted half the spacing between two adjacent filament to A and the 4th to B, a structure different from AABB and ABAB is coined as the FCT structure, because of its resemblance to a face-centered tetragonal unit cell.

Printed mesoporous samples were cured and removed from the substrate upon cooling down to the room temperature. Finally, a capacitor was constructed by sandwiching the 3D-printed PDMS dielectric layer in the middle of two copper-plated PI films with a 3M tape.

C. Characterizations

An IONTOF (TOF-SIMS IV, Münster, Germany) time-of-flight secondary ion mass spectrometry (ToF-SIMS) was

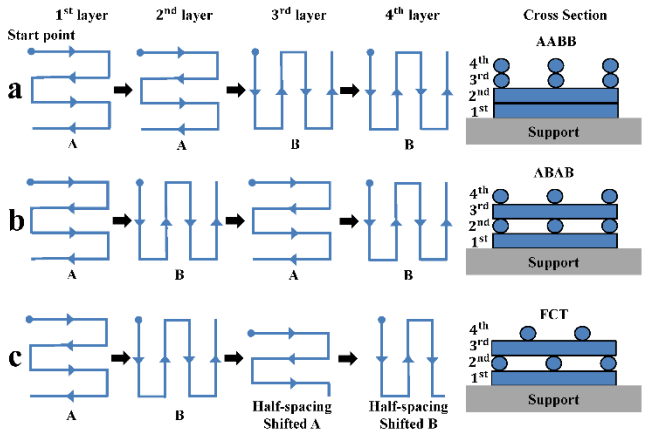

Fig. 2. Illustration showing the printing paths for four layers of meandering PDMS filaments stacked as structures of (a) AABB, (b) ABAB and (c) FCT, as well as their cross section. The term FCT is coined because the cross section of the structure resembles that of a face-centered tetragonal unit cell.

used to analyze the electroless-plated copper layer on a PI film. The 25 keV primary Bi_3^+ cluster ion beam was pulsed at ~1 ns with a target current of ~1 pA, bombarding the surface of the electroless plated copper films. The generated secondary ions were extracted, mass separated and detected via a flight tube and a reflectron-type of time-of-flight analyzer, allowing parallel detection of ions having a mass/charge ratio (m/z) up to ~900 within each cycle (100 μs). The electroless plated copper layers were depth profiled by alternatively sputtering the surface in an area of 200 μm × 200 μm with a 3 keV Cs^+ beam for 1 s (followed by a pause of 0.5 s) and collecting ion mass spectra using the Bi_3^+ primary ion beam at 128 × 128 pixels over an area of 128 μm × 128 μm within the sputtered area. The depths of the craters generated due to the depth profiling were characterized using a profilometer (P-17, KLA-Tencor, USA).

A Zeiss 3D X-ray microscope (Xradia 410 Versa, USA) was used to reveal the structural details of a 3D-printed, FCT-structured, 7-layer PDMS sample. The working principle of the instrument is to reconstruct the (2D) radiographs collected while rotating the sample 360° to assign an intensity value that is responsible to the X-ray absorption at every point in real space (voxel), revealing the structural details. This imaging approach is referred to as computed tomography (CT). Because the instrument is capable of resolving features of microns (the best for this specific instrument under certain conditions is ~1 μm), this technique is commonly referred to as micro-CT. To image the 3D-printed mesoporous dielectric layer, the X-ray source was operated at 60 kV and 133 μA (i.e., 8 W), with a low energy filter (LE5). A 4x objective was used, and both the source-sample and detector-sample distances are 42 mm. With the camera binning of 4, the exposure time of 1 s and projections of 1601, the scanning time was around an hour, and the voxel size was 6.8 μm. In order to observe responses of the filaments of the 3D-printed PDMS structure under pressures, a Deben Microtest *in-situ* testing module (CT500, UK) was used to compress the sample. The micro-CT data were processed using the 2D/3D analysis software Dragonfly Pro (Object Research Systems, Canada).

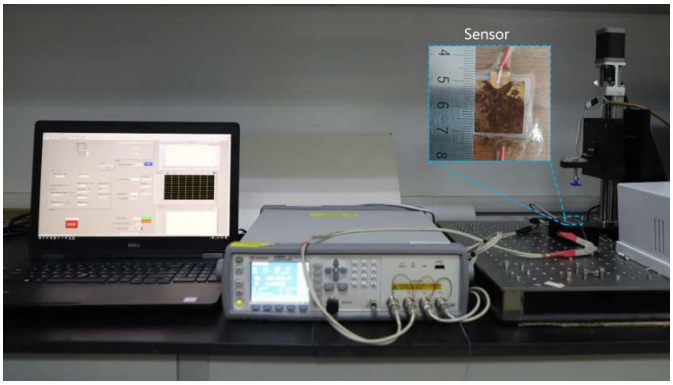

Fig. 3. The capacitance test platform containing pressurizing, capacitance measurement and data acquisition systems. The inset shows a picture of a capacitive sensor with a ruler in centimeter unit.

The PDMS dielectric layers examined had a 4-layer structure, except for the 7-layer one used for micro-CT test. The cross sections of the 3D-printed PDMS mesoporous dielectric layers were examined using a Leica optical microscope. Rheological studies were conducted in a rheometer DHR-2 from TA Instruments. A universal material testing machine (GJ211S, Qing Ji, China) was used for testing the mechanical properties of the 3D-printed PDMS mesoporous structures. Shown in Fig. 3 is the testing platform for evaluating capacitance for the flexible capacitive sensor under pressure, with an E4980A LCR meter (Keysight Technologies, USA) for the measurement of capacitances. The capacitive sensor, along with a pressure head, was attached to a mobile platform with a cantilever dynamometer (SQC-A, Kun Hong, China). When the pressure head started to apply forces on the sensor via direct contact, both the applied force and the changes in capacitance were recorded using home-made software. The inset in the figure shows a picture of a flexible capacitive sensor with a 3D-printed PDMS dielectric layer and two electroless plated copper PI films. The response and recovery time of the capacitive pressure sensors were evaluated with home-made software developed on LabVIEW, with the use of the LCR meter. Investigation on relative changes in capacitance versus radius was conducted by fixing (with the use of an adhesive tape) the sensors against 3D-printed fixtures of Onyx (a composite consisting of engineering nylon and carbon fibers). having radiuses of 20 and 30 mm. A climate-controlled cabinet (KSD-TH-150C9, Dongguan KSAID Testing Instruments, China) was used to examine the relative changes in capacitance of the flexible capacitive sensors as a function of temperature and humidity.

III. Results and Discussion

Shown in Fig. 1 is the process of fabricating a capacitor involving fabrication of flexible electrodes of copper-plated PI films and a 3D-printed dielectric layer of stacked PDMS filaments. Copper was deposited on the PI films via the electroless plating approach [38]. The flexible electrode is compatible with peripheral electronic circuits for future development.

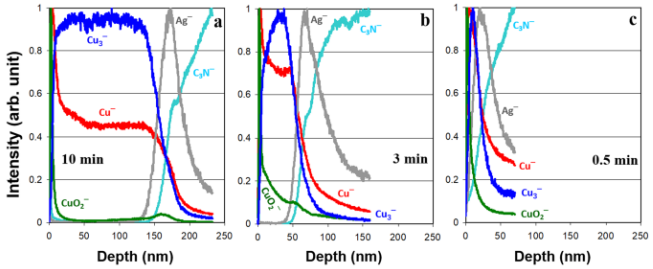

Fig. 4. Depth profiles of copper (represented by Cu^-, Cu_3^-, CuO_2^-), silver (Ag^-) and PI (C_3N^-) for copper plated on a PI film treated by $AgNO_3$ solution for (a) 10, (b) 3, and (c) 0.5 min.

The requirement for the plated copper layer is that it should be thick enough to ensure its conductivity, but not exceeding what is necessary. We have examined the conductivity of copper layers plated on a PI film as a function of plating time. In order to quantify the thickness of a copper layer plated on a PI film, we depth profiled copper layers plated on a PI film by using ToF-SIMS [39].

Shown in Fig. 4 are depth profiles of copper layers plated on a PI film for 10, 3, and 0.5 min. The thickness of the plated copper plated for 10-min is around 150 nm. It is clear that Cu^- is enhanced at the surface due to the existence of the oxide. We noticed that copper clusters Cu_n^-, with Cu_3^- shown in Fig. 4a, are better species to represent the metallic copper layer than Cu^-. The copper oxide layer (CuO_2^-) at the surface of the three samples is on the order of 5 nm. The depth profile of Ag^- shows a silver-containing layer (~40 nm) between the copper layer and the PI film, which is due to the fact that the surface of the PI film (represented by C_3N^-) was catalyzed with a silver nitride solution prior to the copper plating. As shown in Fig. 4b and c, plating times of 3 and 0.5 min are insufficient to make a decent copper layer. Therefore, the depth profiling results shown in Fig. 4 suggest that a plating time of 6-10 min would render a decent copper layer to ensure conductivity.

Fig. 5a shows that the viscosity of the PDMS ink decreases with increasing shear rate, which presents that the PDMS ink possesses a shear-thinning behavior. This behavior means that the fluidity of the ink increases with increasing shear rates, which makes it suitable for printing applications. Fig. 5b shows the results of oscillatory testing carried out to evaluate the viscoelastic properties of the PDMS ink, showing G'>G' at low shear stresses until G' and G" merge and drop vertically (gel point) [35]. This confirms that the ink is predominantly elastic (i.e., solid) at lower shear stresses and becomes liquid-like beyond the gel point. Therefore, the PDMS ink is suitable for 3D printing structures of dielectric layers aiming at constructing capacitive sensors [40].

Fig. 5c presents variations in width of 3D printed PDMS filaments using a 210-μm diameter nozzle as a function of air purging pressure and writing speed. It is clear that the filament width increases with increasing purging pressure and decreasing printing speed. For example, at a higher writing speed of 6 mm/s and lower air purging pressure of 180 kPa, a filament width of ~240 μm was achieved. However, discontinuous filament occurred occasionally in this condition.

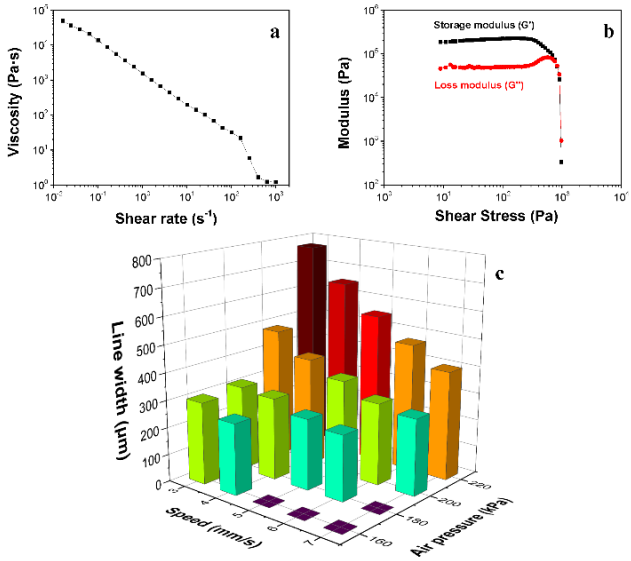

Fig. 5. Rheological property testing results for the PDMS ink, showing (a) apparent viscosity as a function of shear rate and (b) storage modulus G' and loss modulus G" as a function of shear stress. Shown in (c) is the distribution of width in the 3D-printed PDMS filaments using a 210-μm diameter nozzle, as a function of air pressure and writing speed.

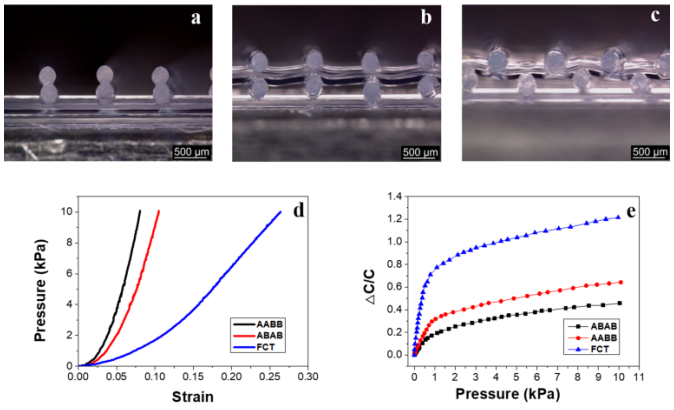

Fig. 6. Photographs of cross sections of DIW 3D-printed PDMS mesoporous dielectric layers with three different structures of (a) AABB, (b) ABAB and (c) FCT. Shown in (d) and (e) are compressive stress-strain curves obtained on the mesoporous dielectric layers and capacitance changes against stress for capacitance sensors constructed using the three structured PMDS layers, respectively.

Furthermore, no continuous filament could be rendered at printing speeds of 5, 6 and 7 mm/s when the air pressure was 160 kPa. The same phenomenon was observed at the printing speed of 7 mm/s and air pressure of 180 kPa. The parameters for 3D printing PDMS structures used in this article, therefore, were determined to be 5 mm/s for printing speed and 180 kPa for air pressure, leaded to thin and continuous filaments with a width of ~260 μm.

Fig. 6a to c show photographs of three 3D-printed cellular PDMS structures of AABB, ABAB and FCT, each containing four layers constructed with printed filaments. The well-defined profiles of the 3D printed PDMS filaments illustrate the excellent structural controllability provided by our DIW technique. Fig. 6d shows that when the same pressure

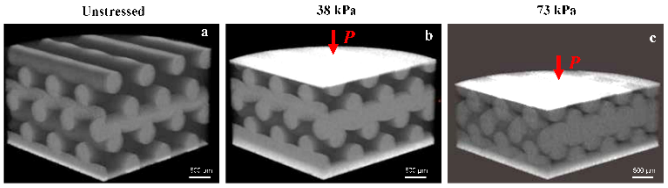

Fig. 7. 3D images rendered from the micro-CT data collected from (a) the unstressed and the stressed 3D-printed, FCT-structured PDMS sample under a pressure (indicated by the inserted arrow) of (b) 38 and (c) 73 kPa.

is applied to the three structures, the deformation of the FCT structure is the largest, followed by the ABAB and the AABB structures. It is thus clear that the effective elastic modulus of the FCT structure is much smaller than that of the other two structures. The differences observed in the effective elastic modulus of the three different structures lies in the fact that the filaments in each layer are stacked quite differently. That is, the filaments in each layer of the FCT structure are staggered, while those in the AABB structure stacked directly within the first and the last two layers. For the ABAB structure, the filaments in each layer stacked every other layer. It is apparent that the three structures of AABB, ABAB and FCT are in decreasing rigidity, just as Fig. 6d suggests.

Fig. 6e shows stress-induced variations in capacitance (ΔC), relative to their unstressed values (C), of the capacitors made of the dielectric layers shown in Fig. 6a to c. Because compressive stress always decreases the distance between the two electrodes, the compressed capacitance is always higher than the unstressed, i.e., $\Delta C > 0$. The slopes of the curves shown in Fig. 6e represent the sensitivity of the capacitors. At the stress range of 0 to 0.4 kPa, $\Delta C/C$ changes approximately linearly with stress. As estimated from Fig. 6e, the sensitivity for capacitors made from FCT, ABAB and AABB structures is 1.23, 0.32, and 0.15 kPa^{-1}, respectively. In other words, the softer the dielectric layer is, the greater the sensitivity. It thus became clear that the elastic modulus of the 3D-printed PDMS structures, as the dielectric layer in a capacitor, dictates the sensitivity of the capacitor. We therefore selected the FCT structure as the design for our 3D-printed PDMS dielectric layer to further investigate how the filament spacing impacts the sensitivity.

The photographs in Fig. 6a to c clearly show the cross section of the 3D-printed PDMS structure; however, understanding the detailed structure, especially its responses to compressive stresses, is required to control the performance of the elastic dielectric layer used for flexible capacitive sensor. This requirement prompted us to take advantage of micro-CT [39], which reveals the structure of an object via different absorption properties of X-ray when it traverses through different materials. Shown in Fig. 7a is a 3D image rendered from the micro-CT data collected for a 3D printed, 7-layer, FCT-structured PDMS sample, with its filament having a diameter of 260 μm and a spacing of 600 μm. The height of the unstressed PDMS sample shown in Fig. 7a is 1548 μm. The sample was placed on the steel stage (which was responsible for the sharper contrast at the bottom of the image) of an *in-situ* testing module capable of compressing

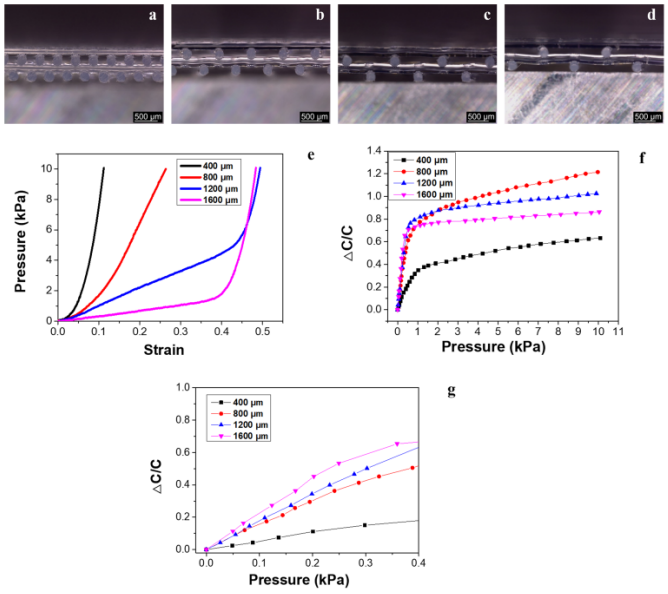

Fig. 8. Photographs showing cross section of the DIW 3D printed PDMS mesoporous dielectric layers with a line spacing of (a) 400, (b) 800, (c) 1200, and (d) 1600 μm. Shown in (e) are stress-strain curves of the above four mesoporous dielectric layers. Shown in (f) are the capacitance sensitivity curves of the capacitors constructed with the four dielectric layers. The capacitance sensitivity in pressure range of 0 to 0.4 kPa is detailed in (g).

the sample. The module was operated at a minimum spacing of 1 mm, not suitable for a 4-layer PDMS sample that is less than 1 mm thick. Therefore, a disk of a 7-layer, FCT-structured PDMS dielectric layer that is taller than 1 mm and has a diameter of 1 cm was used.

Shown in Fig. 7b and c are 3D images rendered from the micro-CT data collected from the same sample, but under a compressive stress of 38 and 73 kPa, respectively, applied via the *in-situ* Deben module. These pressures, which were much higher than those used in the evaluation of stress-strain and capacitance-stress relationships (Fig. 6d and e), were selected to generate large enough strains to be captured by the micro-CT. The compression of the PDMS filaments under pressures is captured by micro-CT imaging. The sharper contrast seen on the top of the images in Fig. 7b and c is the reflection of the physical contacting between the PDMS sample and the top steel block. Under the pressure of 38 (Fig. 7b) and 73 kPa (Fig.7c), the sample height is compressed to 1245 and 971 μm, respectively, which corresponds to a strain of 0.20 and 0.37, respectively. It is clear that micro-CT, combined with an *in-situ* mechanic testing mechanism, is a powerful approach to visualizing and quantifying how the filaments of each layer are squeezed as the compressive stress increases.

Shown in Fig. 8a to d are photographs of four FCT-structured PDMS samples with a filament spacing of 400, 800, 1200, and 1600 μm, respectively. It is expected that smaller spacings yield more rigid structures. This is indeed confirmed by the compressive stress-strain curves shown in Fig. 8e, which can be used to quantify the elasticity of the four structures. For example, to generate a strain of 0.12, it requires a stress of 10.06, 2.38, 1.25, and 0.38 kPa, respectively, for

the PDMS structure with a filament spacing of 400, 800, 1200, and 1600 μm. The slopes of the stress-strain curves of samples with spacings of 1200 and 1600 μm increase drastically when strains reach to 0.44 and 040, respectively. Before this turning point, the elasticity of the two samples can be considered as a composite of PDMS and air voids in the structure. The stress-strain relationship beyond this point should reflect that the filaments have been compressed to a point where PDMS itself mainly determines the elasticity of the two samples. It thus became clear that we can control the elastic properties via the design of 3D-printed PDMS structures to control sensor sensitivity.

Shown in Fig. 8g are variations of $\Delta C/C$ against stress from 0 to 0.4 kPa, where $\Delta C/C$ increases approximately linearly, with its slope representing the highest sensitivity. The highest sensitivity for the capacitors constructed with a PDMS filament spacing of 400, 800, 1200, and 1600 μm is, respectively, 0.37, 1.23, 1.60, and 2.14 kPa^{-1}. As shown in Fig. 8f, the slopes of the curves reduced significantly when the stress is beyond 1 kPa. Though the sensitivity of 1.23 kPa^{-1} is not the largest among the four samples at 0 to 0.4 kPa range, the capacitor constructed with the PDMS structure with the 800-μm spaced filament does have a sensitivity of 0.05 kPa^{-1} at the 1 to 10.3 kPa range. This experimental observation suggests that the 800-μm spacing sample renders an overall best sensitivity in the stress range of 0 to 10 kPa. As a result, we selected the FCT structure with four layers of PDMS filaments having a width of 260 μm, spacing 800 μm in each layer, as the 3D-printed PDMS dielectric layer for capacitive sensors used to examine the device performance. The PDMS layers were 3D printed at a speed of 5 mm/s with a 210-μm nozzle and an extrusion pressure of 180 kPa.

The dielectric constant of the FCT-structured PDMS dielectric layer was measured with an LCR meter by comparing the capacitance with and without the presence of a PDMS sample, which resulted in an effective dielectric constant of 1.21±0.07. This number was surprising at first glance because the dielectric constant for PDMS is 3 [41]. A close examination on the (lack of) contact area between the electrode and the filaments of the PDMS dielectric layer, however, suggested that air has more weight than PDMS on contributing to the effective dielectric constant of the PDMS dielectric layer. Experimental investigation on effective dielectric constant, especially under stresses, for such a complicated composite consisting of air and PDMS will be one of our further research themes.

Shown in Fig. 9a are variations of $\Delta C/C$ against stress, averaged from measuring three capacitors fabricated under the same conditions as the one shown in Fig. 8b (i.e., with a filament spacing of 800 μm, confirming that the DIW 3D printing technology possesses an excellent repeatability for fabricating capacitive sensors. Shown in Fig. 9b were variations of $\Delta C/C$ against stress for a capacitor when it was freshly made and at 2 months old. The results verified that there was no aging effect (at least for the period tested) on the performance of the capacitor. As shown in Fig. 9c, the pressure detection limit of a capacitive sensor was estimated using a weight for manual application and removal of stress. The weight was applied via a needle and a plastic block having an

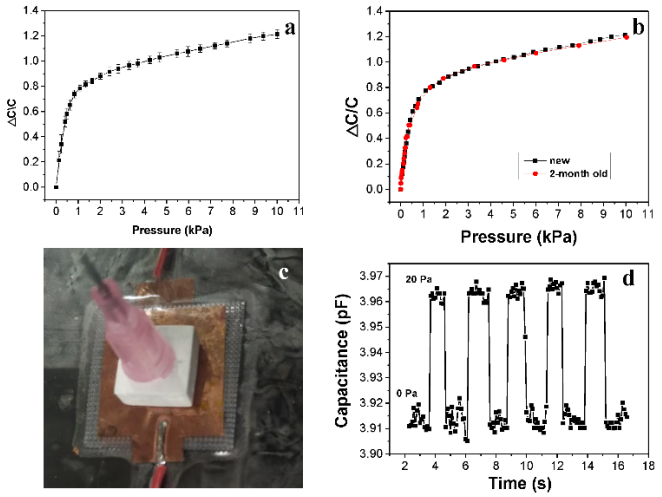

Fig. 9. Repeatability of capacitor performance tested on (a) three FCT samples fabricated under the same conditions (with a PDMS filament spacing of 800 μm) and (b) an FCT sample when it was freshly prepared and stored for two months. The photograph in (c) shows a simple setup for estimating the limit of detection with a weight for a compressive pressure of 20 Pa. Shown in (d) is the response of the capacitor to the placement and removal of the 20-Pa pressure for five times.

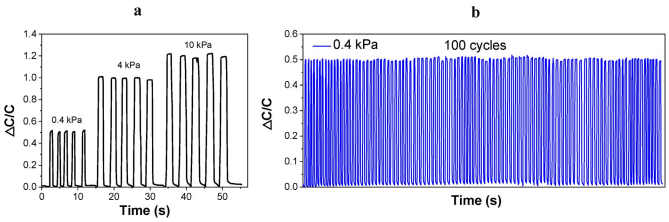

Fig. 10. Capacitance responses to (a) 5 cycles of compressive stresses at 0.4, 4, and 10 kPa and (b) 100 cycles of compressive stress at 0.4 kPa.

area of 100 mm^2, accounting for a total weight of 200 mg or a compressive stress of approximately 20 Pa. Fig. 9d shows capacitances at two well-separated levels of 3.96 to 3.97 and 3.91 to 3.92 pF, corresponding to the placement and removal of the weight, repeated for 5 cycles. The capacitor offered a limit of detection (LoD) better than 20 Pa. A more time-resolved analysis of the capacitance responses to the application and removal of a pressure in Fig. 9d revealed that the transient times for the two actions were 200 and 190 ms, respectively.

A pressure sensor is required to maintain its performance without fatigue failure. Shown in Fig. 10a are capacitance responses to stresses at 0.4, 4, and 10 kPa, cycled five times. No degradation in its sensing performance was observed. As shown in Fig. 10b, we also tested the capacitor at 0.4 kPa for 100 cycles of stressing at 0.4 kPa, confirming that there is no fatigue effect on the sensing performance of the capacitor.

As demonstrated above, our capacitive sensors showed decent sensitivity, LoD and longevity, which ought to offer a great opportunity in applications, such as machine haptics. In such an application, the sensor is required to have robust pressure sensing performance, excellent flexibility and stretchability. Fig. 11 demonstrates the monitoring of force changes in a gripping test with our capacitive sensor. The sensor was

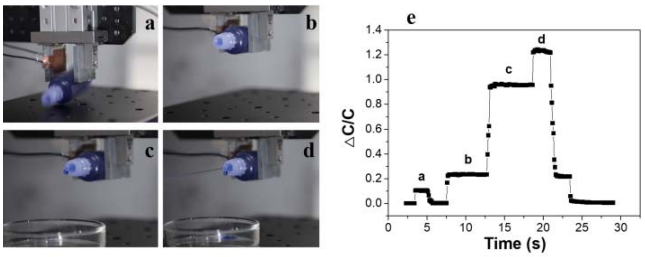

Fig. 11. Images captured from a video recording for a gripping test shows a plastic bottle filled with water dyed with a blue ink at a compression that (a) makes the bottle to fall often, (b) allows the bottle to be gripped steady (c) squeezes water to form a droplet hanging on the nozzle and (d) discharges a stream of water from the nozzle. Shown in (e) are the real-time capacitance changes corresponding to the four compressions shown in (a) to (d).

integrated into a mechanical gripper, whose gripping strength was controlled with compressed air.

Shown in Fig. 11a to d are images captured from a movie (Supplementary Video S1) recording the capturing and squeezing of a 10-ml plastic bottle filled with water dyed with a blue ink (for visual purposes). The four images present responses of the bottle under different compressions, which are monitored via $\Delta C/C$ as shown in Fig. 11e. At a small compression corresponding to $\Delta C/C = 0.1$, the gripper was able to pick up the bottle, but so loosely that the bottle often dropped. For example, Fig. 11a is an image captured from a video showing the falling bottle. When compression became stronger ($\Delta C/C = 0.2$), as shown in Fig. 11b, the bottle was gripped steadily. When the compression increased to the level corresponding to $\Delta C/C = 0.9$, the inked water was squeezed to form a droplet hanging on the nozzle of the bottle (Fig. 11c). As shown in Fig. 11d, a further increased compression corresponding to $\Delta C/C = 1.2$ resulted in a stream of the ink discharging from the bottle. The results demonstrated in Fig. 11 offer an opportunity for applications involving compression, where one can use the electric signal (i.e., capacitance) to control or measure compressive forces.

Summarized in Table I are the performance parameters (sensitivity and LoD) of capacitive pressure sensors and the materials used for the electrodes and the dielectric layers, as well as keywords associated with the fabrication technique for the dielectric layers. This collection of references serves the purpose of comparing different dielectric layer production methodologies. In comparison with the more conventional techniques, such as spin-coating and molding used to prepare dielectric layers for capacitive sensors, our DIW 3D printing approach offers controllability to elasticity and dielectric constant. More importantly, the real strength lies in the scalability of the DIW 3D printing approach, making it especially powerful in commercialization.

As listed in the table, our flexible capacitive sensors, with the dielectric layer fabricated by DIW 3D printing, show reasonably good sensitivity and LoD. With the ability on controlling filament size and porosity in dielectric layers offered by the DIW 3D printing approach demonstrated in this article, it is worth emphasizing that there is a plenty of room for one to achieve sensors tailored to various sensing requirements.

TABLE I
SUMMARY OF MATERIAL SELECTION AND FABRICATING METHODOLOGIES FOR DIELECTRIC LAYER AND ELECTRODE OF CAPACITIVE SENSORS AND THEIR SENSITIVITY AND LOD

Dielectric (process)	Electrode	Sensitivity (kPa^{-1})	LoD (Pa)	Ref.
PDMS (mold, dissolve)	Conductive fabric	0.0121(up to 100 kPa)	N.A.	27
PET (fabrics)	Carbon fiber bundles	0.045 (0-10 kPa)	N.A.	19
Ag-PDMS (coat, degas)	indium-tin-oxide (ITO)-covered glass cell	0.11 (<1 kPa)	8	16
PDMS (coat, dissolve)	silver nanoparticles deposited styrene-block-but adiene-styrene	0.278 (<2 kPa)	38.83	15
PDMS (mold)	indium tin oxide-coated PET	0.55 (<2 kPa)	3	12
PDMS (spin-coat)	Au thermally evaporated PEN	0.55-0.58 (N.A.)	N.A.	21
PS (spin-coat)	Spin-coating micropatterned PDMS/Au	0.815 (N.A.)	17.5	24
Fluorosilicone (spin-coat)	Copper/tin coated woven fabric	0.91 (<0.5 kPa)	500	2
PDMS (evaporate)	indium tin oxide-coated PET	1.18 (<0.02 kPa)	N.A.	14
Natural Plants	AgNW sprayed on Colorless polyacetimidate	1.54 (<1 kPa)	0.6	30
PDMS (mold)	indium tin oxide-coated PET	1.62 (<0.2 kPa)	3	26
PDMS (mold)	Screen printed PET/Ag	2.21 (0-100 Pa)	N.A.	20
PMMA/PVP (spin-coat)	AgNW bar-coated PDMS with buckled surface	3.8 (45-500 Pa)	15	25
Carbon black/PDMS (water-in-oil emulsion)	Copper tape	35 (0-0.2 kPa)	8.8	29
PDMS (mold)	indium tin oxide-coated PET	44.5 (<100 Pa)	0.14	18
PDMS (direct ink write)	Copper-plated polyimide	1.23 (0-0.4 kPa)	20	This work

Applications of flexible sensors will inevitably introduce deformations. One of the deformations, bending, of our capacitive sensor was examined. Shown in Fig. 12 are the changes of the capacitance of a capacitive sensor relative to its value without bending. The sensor was bent via its fixation to 3D printed round structures having a radius of 20 and 30 mm using a double-sided adhesive tape. When the sensor was bent, its capacitance increased with increasing bending (i.e., decreasing bending radius). The increase capacitance due to bending is believed to be cause by a decreased distance between the two electrodes.

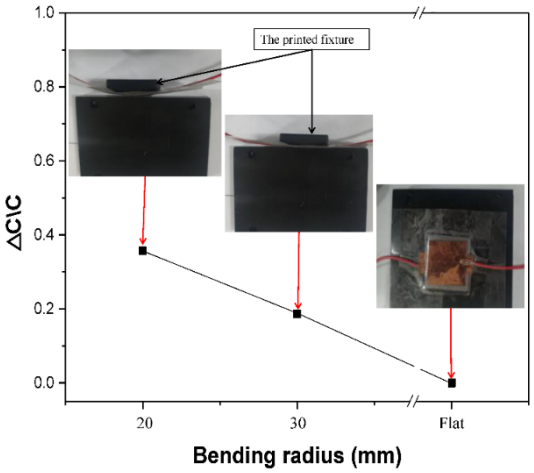

Fig. 12. Capacitance changes induced by bending, relative to its value without bending, via its fixation onto 3D printed structures with a radius of 20 and 30 mm.

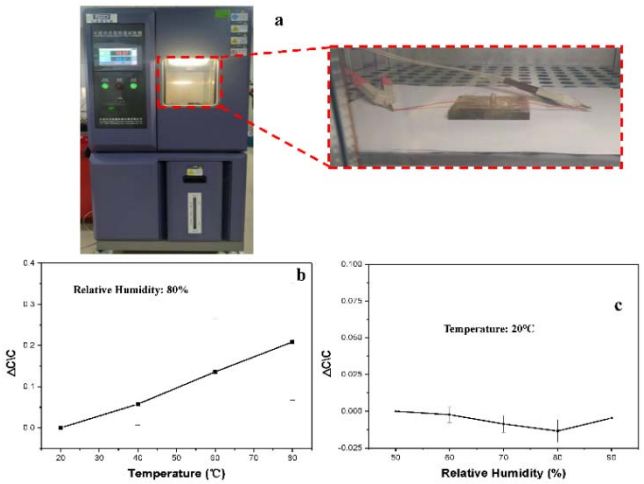

Fig. 13. The climate-controlled chamber (a) used to investigate the response of a capacitive sensor to (b) temperature and (c) humidity.

The climate-controlled setup for understanding changes in capacitance of sensors is shown in Fig. 13a. The inset is the detailed view of the sample through the view window. The test was carried out under a pressure provided with a weight of 2 g. The changes in capacitance of the capacitor at 40, 60, and 80 °C, relative to that at 20 °C, are shown in Fig. 13b. For this temperature testing, the relative humidity was fixed at 80%. Capacitance was observed to increase with increasing temperature. For example, at 80 °C the capacitance increased 20% from that at 20 °C. The experimental results may be explained by pressures generated as the thermal response of the adhesive tape, which was used to attach the flexible electrodes to the PDMS dielectric layer. By contrast, as shown in Fig. 13c, the capacitances measured at 20 °C and at relative humidity of 50%, 60%, 70%, 80%, and 90% were quite similar to each other, confirming that the sensor is insensitive to humidity.

Our primitive experimental setup for bending and climate-controlled tests allowed us to measure capacitance without being able to apply pressures to measure the sensitivity of the sensors. A complete testing system is being built in our group, which is expected to contribute to evaluating sensor performance under various conditions.

IV. Conclusion

We have developed highly sensitive, flexible capacitive sensors having an elastomeric dielectric layer of 3D-printed mesoporous PDMS sandwiched between two electrodes of electroless copper plated PI films. The mesoporous structure of PDMS was built via the direct ink writing approach, which allows 3D printing of layers consisting of PDMS filaments. The elasticity of those mesoporous structures was not only determined by the size of spacing between the PDMS filaments within each layer, but also the alignment of filaments of each layer relative to its adjacent layers. The response of the capacitance of our flexible capacitive sensors to compressive stresses is affected by the elasticity of the PDMS dielectric structure.

By investigating the compressive stress-strain behaviors and the capacitance changes versus stress, it was found that the FCT structure of four staggered layers of 260-μm-diameter filaments with a spacing of 800 μm renders an overall superior sensitivity in the pressure range of 0 to 10 kPa (with a sensitivity of 1.23 kPa^{-1} at the low end of the pressure range) and a limit of detection better than 20 Pa. We confirmed the reproducibility, repeatability and longevity of our capacitive sensors, as well as demonstrated an application where a sensor was used to control the force of a mechanical gripper. With controllable effective elastic modulus and dielectric constant via structured PDMS filaments acting as a composite of air and PDMS, our flexible capacitive sensors are expected to be widely applied in haptic technologies.

References

[1] N. Lu and D.-H. Kim, "Flexible and stretchable electronics paving the way for soft robotics," *Soft Robot.*, vol. 1, no. 1, pp. 53–62, Mar. 2014.
[2] L. Viry *et al.*, "Flexible three-axial force sensor for soft and highly sensitive artificial touch," *Adv. Mater.*, vol. 26, no. 17, pp. 2659–2664, May 2014.
[3] Y. Huang, D. Fang, C. Wu, W. Wang, X. Guo, and P. Liu, "A flexible touch-pressure sensor array with wireless transmission system for robotic skin," *Rev. Sci. Instrum.*, vol. 87, no. 6, Jun. 2016, Art. no. 065007.
[4] N. C. Sears, J. D. Berrigan, P. R. Buskohl, and R. L. Harne, "Dynamic response of flexible hybrid electronic material systems," *Compos. Struct.*, vol. 208, pp. 377–384, Jan. 2019.
[5] Q. Hua *et al.*, "Skin-inspired highly stretchable and conformable matrix networks for multifunctional sensing," *Nature Commun.*, vol. 9, no. 1, pp. 1–11, Jan. 2018.
[6] Y. Zang, F. Zhang, C.-A. Di, and D. Zhu, "Advances of flexible pressure sensors toward artificial intelligence and health care applications," *Mater. Horizons*, vol. 2, no. 2, pp. 140–156, Mar. 2015.
[7] T. Someya, T. Sekitani, S. Iba, Y. Kato, H. Kawaguchi, and T. Sakurai, "A large-area, flexible pressure sensor matrix with organic field-effect transistors for artificial skin applications," *Proc. Nat. Acad. Sci. USA*, vol. 101, no. 27, pp. 9966–9970, Jul. 2004.
[8] T. Yamada *et al.*, "A stretchable carbon nanotube strain sensor for human-motion detection," *Nature Nanotechnol.*, vol. 6, no. 5, pp. 296–301, May 2011.
[9] C.-L. Choong *et al.*, "Highly stretchable resistive pressure sensors using a conductive elastomeric composite on a micropyramid array," *Adv. Mater.*, vol. 26, no. 21, pp. 3451–3458, Jun. 2014.
[10] J. A. Dobrzynska and M. A. M. Gijs, "Flexible polyimide-based force sensor," *Sens. Actuators A, Phys.*, vol. 173, no. 1, pp. 127–135, Jan. 2012.

[11] H. B. Muhammad *et al.*, "A capacitive tactile sensor array for surface texture discrimination," *Microelectron. Eng.*, vol. 88, no. 8, pp. 1811–1813, Aug. 2011.
[12] S. C. B. Mannsfeld *et al.*, "Highly sensitive flexible pressure sensors with microstructured rubber dielectric layers," *Nature Mater.*, vol. 9, no. 10, pp. 859–864, Oct. 2010.
[13] M. L. Hammock, A. Chortos, B. C.-K. Tee, J. B.-H. Tok, and Z. A. Bao, "25th anniversary article: The evolution of electronic skin (E-skin): A brief history, design considerations, and recent progress," *Adv. Mater.*, vol. 25, no. 42, pp. 5997–6037, Nov. 2013.
[14] B.-Y. Lee, J. Kim, H. Kim, C. Kim, and S.-D. Lee, "Low-cost flexible pressure sensor based on dielectric elastomer film with micro-pores," *Sens. Actuators A, Phys.*, vol. 240, pp. 103–109, Apr. 2016.
[15] A. Chhetry, H. Yoon, and J. Y. Park, "A flexible and highly sensitive capacitive pressure sensor based on conductive fibers with a microporous dielectric for wearable electronics," *J. Mater. Chem. C*, vol. 5, no. 38, pp. 10068–10076, Oct. 2017.
[16] S.-Y. Liu, J.-G. Lu, and H.-P.-D. Shieh, "Influence of permittivity on the sensitivity of porous elastomer-based capacitive pressure sensors," *IEEE Sensors J.*, vol. 18, no. 5, pp. 1870–1876, Mar. 2018.
[17] S. Kang *et al.*, "Highly sensitive pressure sensor based on bioinspired porous structure for real-time tactile sensing," *Adv. Electron. Mater.*, vol. 2, no. 12, Dec. 2016, Art. no. 1600356.
[18] J. C. Yang *et al.*, "Microstructured porous pyramid-based ultrahigh sensitive pressure sensor insensitive to strain and temperature," *ACS Appl. Mater. Interfaces*, vol. 11, no. 21, pp. 19472–19480, May 2019.
[19] S. Li, R. Li, T. Chen, and X. Xiao, "Highly sensitive and flexible capacitive pressure sensor enhanced by weaving of pyramidal concavities staggered in honeycomb matrix," *IEEE Sensors J.*, vol. 20, no. 23, pp. 14436–14443, Dec. 2020.
[20] V. Palaniappan *et al.*, "Laser-assisted fabrication of a highly sensitive and flexible micro pyramid-structured pressure sensor for E-skin applications," *IEEE Sensors J.*, vol. 20, no. 14, pp. 7605–7613, Jul. 2020.
[21] C. Pang *et al.*, "Highly skin-conformal microhairy sensor for pulse signal amplification," *Adv. Mater.*, vol. 27, no. 4, pp. 634–640, Jan. 2015.
[22] J. Park *et al.*, "Tactile-direction-sensitive and stretchable electronic skins based on human-skin-inspired interlocked microstructures," *ACS Nano*, vol. 8, no. 12, pp. 12020–12029, Dec. 2014.
[23] Y. Xiong *et al.*, "A flexible, ultra-highly sensitive and stable capacitive pressure sensor with convex microarrays for motion and health monitoring," *Nano Energy*, vol. 70, Apr. 2020, Art. no. 104436.
[24] T. Li *et al.*, "Flexible capacitive tactile sensor based on micropatterned dielectric layer," *Small*, vol. 12, no. 36, pp. 5042–5048, Sep. 2016.
[25] Y. Joo *et al.*, "Silver nanowire-embedded PDMS with a multiscale structure for a highly sensitive and robust flexible pressure sensor," *Nanoscale*, vol. 7, no. 14, pp. 6208–6215, 2015.
[26] B. Zhuo, S. Chen, M. Zhao, and X. Guo, "High sensitivity flexible capacitive pressure sensor using polydimethylsiloxane elastomer dielectric layer micro-structured by 3-D printed mold," *IEEE J. Electron Devices Soc.*, vol. 5, no. 3, pp. 219–223, May 2017.
[27] O. Atalay, A. Atalay, J. Gafford, and C. Walsh, "A highly sensitive capacitive-based soft pressure sensor based on a conductive fabric and a microporous dielectric layer," *Adv. Mater. Technol.*, vol. 3, no. 1, Jan. 2018, Art. no. 1700237.
[28] H.-B. Yao *et al.*, "A flexible and highly pressure-sensitive graphene-polyurethane sponge based on fractured microstructure design," *Adv. Mater.*, vol. 25, no. 46, pp. 6692–6698, Dec. 2013.
[29] M. Pruvost, W. J. Smit, C. Monteux, P. Poulin, and A. Colin, "Polymeric foams for flexible and highly sensitive low-pressure capacitive sensors," *npj Flexible Electron.*, vol. 3, no. 1, pp. 1–6, Dec. 2019.
[30] Y. Wan *et al.*, "Natural plant materials as dielectric layer for highly sensitive flexible electronic skin," *Small*, vol. 14, no. 35, Aug. 2018, Art. no. 1801657.
[31] S. K. Saha, D. Wang, V. H. Nguyen, Y. Chang, J. S. Oakdale, and S.-C. Chen, "Scalable submicrometer additive manufacturing," *Science*, vol. 366, no. 6461, pp. 105–109, Oct. 2019.
[32] M. A. Skylar-Scott, J. Mueller, C. W. Visser, and J. A. Lewis, "Voxelated soft matter via multimaterial multinozzle 3D printing," *Nature*, vol. 575, no. 7782, pp. 330–335, Nov. 2019.
[33] Q. Sun, Z. Yang, H. Cheng, Y. Peng, Y. Huang, and M. Chen, "Creation of three-dimensional structures by direct ink writing with kaolin suspensions," *J. Mater. Chem. C*, vol. 6, no. 42, pp. 11392–11400, Nov. 2018.
[34] A. Chortos, E. Hajiesmaili, J. Morales, D. R. Clarke, and J. A. Lewis, "3D printing of interdigitated dielectric elastomer actuators," *Adv. Funct. Mater.*, vol. 30, no. 1, Jan. 2020, Art. no. 1907375.
[35] Q. Chen, P.-F. Cao, and R. C. Advincula, "Mechanically robust, ultra-elastic hierarchical foam with tunable properties via 3D printing," *Adv. Funct. Mater.*, vol. 28, no. 21, May 2018, Art. no. 1800631.
[36] E. B. Duoss *et al.*, "Three-dimensional printing of elastomeric, cellular architectures with negative stiffness," *Adv. Funct. Mater.*, vol. 24, no. 31, pp. 4905–4913, Aug. 2014.
[37] Z. Wang *et al.*, "3D-printed graphene/polydimethylsiloxane composites for stretchable and strain-insensitive temperature sensors," *ACS Appl. Mater. Interfaces*, vol. 11, no. 1, pp. 1344–1352, Jan. 2019.
[38] W.-R. Cai *et al.*, "Fabrication of copper electrode on flexible substrate through Ag^{+}-based inkjet printing and rapid electroless metallization," *IEEE Trans. Compon., Packag., Manuf. Technol.*, vol. 7, no. 9, pp. 1552–1559, Sep. 2017.
[39] L. Du *et al.*, "Time-of-flight secondary ion mass spectrometry analyses of vancomycin," *Biointerphases*, vol. 13, no. 3, May/Jun. 2018, Art. no. 03B401.
[40] A. D. Plessis, I. Yadroitsev, I. Yadroitsava, and S. G. Le Roux, "X-ray microcomputed tomography in additive manufacturing: A review of the current technology and applications," *3D Printing Additive Manuf.*, vol. 5, no. 3, pp. 227–247, Sep. 2018.
[41] *Dielectric Constant for DOWSIL SE 1700 Is Listed*. Accessed: Dec. 2017. [Online]. Available: https://www.dow.com/en-us/pdp.dowsil-se-1700.01707116z.html

Wenzhen Yang received the B.S. degree from the College of Computer and Information Science, Southwest University, Chongqing, China, in 2012. He is currently pursuing the Ph.D. degree with the School of Mechanical Engineering, Jiangnan University. His research interests include 3-D printing, soft electronics, and wearable sensors.

Yu Liu received the B.S degree in control science and engineering from the Harbin Institute of Technology, Harbin, China, the M.S. degree in mechanical engineering from Kyungpook National University, Daegu, South Korea, and the Ph.D. degree from the University of Western Ontario, London, ON, Canada. He is currently a Professor and a Vice-President with the School of Mechanical Engineering, Jiangnan University, Wuxi, China. He has authored over 80 peer-reviewed literature publications and three book chapters, and holds more than 60 patents, including 40 registered U.S. patents. His current research interests include additive manufacturing, 3-D printed electronics, precision mechatronics, and micro/nano manufacturing. He is leading the Institute of Precision Intelligent System Engineering (iPISE) for establishing optimal solutions to the emerging 3-D mechatronics. iPISE has quickly developed, through having interacted with doses of local partners and built its increasing local impact on 3-D printed electronics and direct fabrication, especially on equipment and instrumentation and control.

Wei Xu received the bachelor's and master's degrees in mechanical engineering from Jiangnan University, Wuxi, China. He currently works as an Engineer with Schneider Electric, Wuxi. His research interests include 3-D printing, micro-CT, and wearable sensors. He carried our research work on using micro-CT to evaluate 3-D-printed elastomer structures at Surface Science Western, The University of Western Ontario, Canada, in 2020, as a Visiting Graduate Student.

Heng-Yong Nie received the bachelor's degree in engineering (solid state devices) from the University of Electronic Science and Technology of China in 1984, and the master's degree in engineering (electronic materials) and the Ph.D. degree in engineering (materials science) from the University of Tsukuba, Japan, in 1988 and 1992, respectively. He worked as a National Institute Postdoctoral Fellow with the National Institute for Advanced Interdisciplinary Research, Tsukuba, from 1992 to 1995 and a Research Associate with the Yokohama Research Center of Mitsubishi Chemical Corporation from 1995 to 1997. He joined Surface Science Western (SSW) in 1997. He is currently a Research Scientist with SSW, The University of Western Ontario, Canada, and also an Adjunct Research Professor with the Department of Physics and Astronomy, The University of Western Ontario. In addition to providing consultancy to industrial partners on failure analyses related to surface chemistry and processing, his research focuses are in developing analytical approaches to studying soft materials, mainly using time-of-flight secondary ion mass spectrometry and atomic force microscopy. He carries out research on formation mechanisms of self-assembled monolayers (SAMs) on metal oxides and their applications in surface engineering.